

Photo-electron momentum spectra from minimal volumes: the time-dependent surface flux method

Liang Tao^{1,2} and Armin Scrinzi¹

¹Ludwig Maximilians Universität, Theresienstrasse 37, 80333 Munich, Germany

²Wolfgang Pauli Institute c/o University of Vienna, Nordbergstrasse 15, 1090 Vienna, Austria

E-mail: armin.scrinzi@lmu.de

Abstract. The time-dependent surface flux (t-SURFF) method is introduced for computing of strong-field infrared photo-ionization spectra of atoms by numerically solving the time-dependent Schrödinger equation on minimal simulation volumes. The volumes only need to accommodate the electron quiver motion and the relevant range of the atomic binding potential. Spectra are computed from the electron flux through a surface, beyond which the outgoing flux is absorbed by infinite range exterior complex scaling (irECS). Highly accurate infrared photo-electron spectra are calculated in single active electron approximation and compared to literature results. Detailed numerical evidence for performance and accuracy is given. Extensions to multi-electron systems and double ionization are discussed.

1. Introduction

In a broad range of recent experiments, strong infrared laser pulses, often combined with high harmonic pulses, are used to study the electronic dynamics of atoms and molecules on the natural time scale of valence electron motion of $\lesssim 1 fs$. Basic mechanisms of the IR-electron interaction are well understood within the simple semi-classical re-collision model [1], but for a more detailed understanding numerical simulations must be employed. This is due to the fundamentally non-perturbative interaction of near IR fields with valence electrons at intensities of $\gtrsim 10^{14} W/cm^2$. Even for the simplest single-electron models the simulation remains challenging, especially when accurate photo-electron momentum spectra are required, as, e.g., for re-collision imaging [2, 3, 4]. When two-electron processes are involved, one quickly reaches the limits of present day computer resources [5, 6].

The surprising difficulty in simulating a seemingly simple process like ionization by a dipole field is due to the presence of vastly different length- and time-scales: first, even though the laser pulses can be as short as a single optical cycle, at the Ti:Sapphire wave length of $\lambda = 800 nm$ this still corresponds to a FWHM duration of $\gtrsim 2.5 fs$ or about 110 atomic units (a.u., $\hbar = e^2 = m_e = 1$). During that time, a photo-electron with an energy of $13 eV \approx 1/2 a.u.$ moves to a distance of ≈ 110 Bohr, which sets a lower limit for the required box-size, if reflections from box boundaries are to be avoided. In practice, higher energies and longer pulse durations including the rise and fall of the pulses are of interest, leading to simulation volumes with diameters of thousands of atomic units. At the same time, photo-electron spectra are broad, extending to at least $2U_p$ for the “direct” photo-electrons and further up to about $10U_p$ for the “re-scattered” electrons. Re-scattered electrons are those that after ionization re-directed to the nucleus by the laser field, where they absorb more photons in an inelastic scattering process. The ponderomotive potential $U_p = I/(4\omega^2)$ grows linearly with laser intensity I and quadratically with wavelength. At the moderate intensity $I = 10^{14} W/cm^2$ and $\lambda = 800 nm$ it is $U_p = 0.22 a.u. \approx 6 eV$. The re-scattering momentum energy cutoff of $10U_p$ corresponds to a photo-electron momentum of $2.2 a.u.$ For representation of such momenta on a spatial grid, we need grid spacings of at least $\Delta x \lesssim 2\pi/2 a.u.$, for accurate results usually significantly more than this. This leaves us with thousands of grid points in each spatial direction even for moderate laser parameters. The situation quickly worsens at higher intensities and longer wavelengths.

This general requirement on discretization cannot be overcome by any specific representation of the wave function: speaking in terms of classical mechanics, we must represent the phase space that is covered by the electrons, which involves a certain range of momenta and positions. If we have no additional knowledge of the structure of solution, the number of discretization points we need is the phase space volume divided by the Planck constant h . In some cases like, for example, single-photon ionization, we can exploit the fact that at long distances the solution covers only a very narrow range of momenta and only the spatially well-localized initial bound state requires a

broader range of momenta: the phase-space volume remains small, simple models like perturbation theory allow reproducing the physics. We have no such simplifying physical insight for strong-field IR photo-ionization.

The lower limit for the number of discretization points for the complete wave function can be approached by different strategies: the choice of velocity gauge [7], working in the Kramers-Henneberger frame [8] or in momentum space [9], by variable grid spacings, or by expanding into time-dependent basis functions [10]. A promising strategy is to follow the solution in time [11].

Alternatively, we can abandon the attempt of representing the complete wave-function and instead use absorbing boundaries and extract momenta at finite distances. The time-dependent surface flux method (t-SURFF) introduced here is such an approach. After its mathematical derivation, numerical implementation is briefly discussed. Angle-resolved photo-electron spectra are presented using between 75 and 200 radial discretization points for truncated and full Coulomb potentials. We discuss accuracies and demonstrate the efficiency of t-SURFF by comparison with recent literature. Finally, possible extensions to few-electron systems and double photo-electron spectra are outlined.

2. The t-SURFF method

Scattering measurements and theory are both based on the plausible idea that interactions are limited to finite ranges in space and time and that at large times $> T$ and large distances $> R$ the time-evolution of the scattering particle is that of free motion:

$$\Psi(\vec{r}, t) \sim \int dk^{(3)} \exp(-it\vec{k}^2/2)b(\vec{k})\chi_{\vec{k}}(\vec{r}) \quad \text{for } t > T, |\vec{r}| > R, \quad (1)$$

where $\chi_{\vec{k}}(\vec{r}) = (2\pi)^{-3/2} \exp(i\vec{k} \cdot \vec{r})$ are δ -normalized plane waves. The measured momentum spectrum is proportional to the square of the spectral amplitudes $b(\vec{k})$

$$\sigma(\vec{k}) \propto |b(\vec{k})|^2. \quad (2)$$

For Hamiltonians that are time-independent beyond a certain time T , we can readily obtain the spectral amplitudes $b(\vec{k})$ by decomposing the wave function $\Psi(\vec{r}, T)$ into its spectral components

$$b(\vec{k}) = \langle \psi_{\vec{k}} | \Psi(T) \rangle \exp(-iT\vec{k}^2/2), \quad (3)$$

where the scattering solutions

$$H(T)|\psi_{\vec{k}}\rangle = \frac{\vec{k}^2}{2}|\psi_{\vec{k}}\rangle \quad (4)$$

have the asymptotic behavior

$$\psi_{\vec{k}}(\vec{r}) \sim \chi_{\vec{k}}(\vec{r}) \quad \text{for } |\vec{r}| \rightarrow \infty. \quad (5)$$

For computing $b(\vec{k})$, one needs to (i) propagate a solution $\Psi(\vec{r}, t)$ until time T , (ii) obtain the scattering solutions $\psi_{\vec{k}}$. Unfortunately, both of these tasks are non-trivial

in all but the simplest cases. As discussed above, solving the TDSE with IR fields is numerically challenging because of the large box sizes needed. “Obtaining the scattering solution” amounts to outright solving a time-independent scattering problem for $H(T)$, but analytic scattering wave functions are only known for simple model potentials and for the Coulomb potential.

Rather than letting the system evolve and analyzing it at the end of the evolution, we can record the particle flux leaving a finite volume as the systems evolves. Such a procedure neither requires stationary scattering solutions nor the complete wave function in an asymptotically large volume. It is practical, if we either know the further time-evolution of the system outside the finite volume in analytic form or if it can be obtained with little numerical effort. This type of methods has been applied for reactive scattering with time-independent Hamiltonians [12, 13], where obtaining scattering solutions would be tantamount to solving the complete stationary scattering problem, a daunting task for few-body systems.

Photo-ionization cannot be computed by existing surface flux methods, as the dipole interaction is non-local and the external field modifies the particle energies everywhere, in particular also after the particle has left the finite simulation volume. To handle this, we have developed the time-dependent surface flux (t-SURFF) method, that will be derived in the following. A preliminary version of the method was published in [14].

Let us choose a surface radius R_c large enough that the particle motion can be considered a free motion and that all occupied bound states of the system have negligible particle density at $|\vec{r}| > R_c$. Let us further pick a sufficiently large time T such that all particles that will ever reach our detector with energy $\vec{k}^2/2 > 0$ are outside the finite volume $|\vec{r}| < R_c$. At that time, the wave function has split into bound and asymptotic parts

$$\Psi(\vec{r}, T) = \Psi_b(\vec{r}, T) + \Psi_s(\vec{r}, T) \quad (6)$$

with

$$\Psi_b(\vec{r}, T) \approx 0 \quad \text{for } |\vec{r}| \geq R_c \quad (7)$$

$$\Psi_s(\vec{r}, T) := \int dk^{(3)} \exp(-iT\vec{k}^2/2)b(\vec{k})\psi_{\vec{k}}(\vec{r}) \approx 0 \quad \text{for } |\vec{r}| \leq R_c. \quad (8)$$

The approximate sign in (8) refers to the fact that very low energy particles $\vec{k}^2/2 \sim 0$ may not have left the finite volume at time T . It follows that, the lower the energy, the larger T will be required for the splitting to hold. Although each individual $\chi_{\vec{k}}$ extends over the complete space, the scattering wave-packet is localized outside R_c up to a small error that quickly decays with growing T . The scattering amplitudes $b_{\vec{k}}$ can be obtained as

$$e^{iT\vec{k}^2/2}b(\vec{k}) = \langle \psi_k | \Psi_s(T) \rangle \approx \langle \psi_k | \theta(R_c) | \Psi_s(T) \rangle = \langle \chi_k | \theta(R_c) | \Psi_s(T) \rangle. \quad (9)$$

Here we introduced the notation

$$\langle \psi_k | \theta(R_c) | \Psi_s(T) \rangle := \int_{|\vec{r}| > R_c} d^{(3)}r \psi_{\vec{k}}^*(\vec{r}) \Psi_s(\vec{r}, T) \quad (10)$$

The substitution of the scattering solution with a plane wave $\psi_{\vec{k}} \rightarrow \chi_{\vec{k}}$ in the last step uses the asymptotic behavior (5). It is exact, when all interactions vanish beyond R_c .

For converting the above matrix element to a time-integral over surface values, we must assume that we know the time-evolution of the particle *after it has passed through the surface*. For that we assume that there is a ‘‘channel Hamiltonian’’ $H_c(t)$ such that

$$H_c(t) = H(t) \quad \text{for } |\vec{r}| > R_c \text{ and } \forall t. \quad (11)$$

In case of a short range potential $V(\vec{r}) \equiv 0$ for $|\vec{r}| > R_c$ this is *exactly* fulfilled by the Hamiltonian for the free motion in the laser field

$$H_c(t) = \frac{1}{2}[-i\vec{\nabla} - \vec{A}(t)]^2, \quad (12)$$

where $\vec{A}(t) = -\int_{-\infty}^t \vec{\mathcal{E}}(t')dt'$ for the dipole field $\vec{\mathcal{E}}(t)$. The Volkov solutions

$$\chi_{\vec{k}}(\vec{r}) = (2\pi)^{-3/2} e^{-i\Phi(\vec{k},t)} e^{i\vec{k}\cdot\vec{r}}, \quad \Phi(\vec{k},t) = \frac{1}{2} \int_0^t d\tau [\vec{k} - \vec{A}(\tau)]^2 \quad (13)$$

solve the TDSE

$$i \frac{d}{dt} |\chi_{\vec{k}}(t)\rangle = H_c(t) |\chi_{\vec{k}}(t)\rangle. \quad (14)$$

We can now write

$$\begin{aligned} \langle \chi_k(T) | \theta(R_c) | \Psi_s(T) \rangle &= \int_0^T dt \frac{d}{dt} \langle \chi_k(t) | \theta(R_c) | \Psi_s(t) \rangle \\ &= i \int_0^T dt \langle \chi_k(t) | H_c(t) \theta(R_c) - \theta(R_c) H(t) | \Psi_s(t) \rangle \\ &= i \int_0^T dt \langle \chi_k(t) | \left[-\frac{1}{2} \Delta + i \vec{A}(t) \cdot \vec{\nabla}, \theta(R_c) \right] | \Psi_s(t) \rangle \end{aligned} \quad (15)$$

The commutator vanishes everywhere except on the surface $|\vec{r}| = R_c$. Assuming linear polarization in z -direction $\vec{A}(t) = (0, 0, A(t))$, it can be written in polar coordinates (r, θ, ϕ) as

$$\begin{aligned} \left[-\frac{1}{2} \Delta + i A(t) \partial_z, \theta(R_c) \right] &= \\ &= -\frac{1}{2} r^{-2} \partial_r r^2 \delta(r - R_c) - \frac{1}{2} \delta(r - R_c) \partial_r - i A(t) \cos \theta \delta(r - R_c) \end{aligned} \quad (16)$$

With this, the volume integral over the space covered by the solution at time T has been converted to a time-integral up to T and a surface integral over $|\vec{r}| = R_c$.

We would like to remark that without time-dependence we can make one more step, as then the Volkov phase reduces to $\Phi(\vec{k}, t) = t\vec{k}^2/2$ and time-integration turns into the time-energy Fourier-transform of the surface integral, which connects to the well-known results of, e.g., Ref. [13].

3. Finite element discretization and irECS

For the efficient use of t-SURFF, a reliable mechanism for truncating the solution outside the finite volume without generating reflections or other artefacts is needed. Commonly complex absorbing potentials are employed for that purpose (for a recent review, see [15]). We use infinite range exterior scaling (irECS) introduced and discussed in detail in reference [16]. Here we only briefly summarize the procedure.

Exterior complex scaling (ECS) consists in making an analytic continuation of the Hamiltonian by rotating the coordinates into the upper complex plane beyond the “scaling radius” R_0 :

$$\vec{r} \rightarrow \vec{r}_{\theta R_0} = \begin{cases} \vec{r} & \text{for } |\vec{r}| \leq R_0 \\ \frac{\vec{r}}{|\vec{r}|} [R_0 + e^{i\theta}(|\vec{r}| - R_0)] & \text{for } |\vec{r}| > R_0 \end{cases} \quad (17)$$

The resulting complex scaled Hamiltonian $H_{\theta R_0}$ can be used in a complex scaled time-dependent Schrödinger equation

$$i \frac{d}{dt} \Psi_{\theta R_0}(t) = H_{\theta R_0}(t) \Psi_{\theta R_0}(t). \quad (18)$$

It was observed in [16] that for the velocity form of the TDSE, in the unscaled region $|\vec{r}| < R_0$ exact and complex scaled solution agree: $\Psi_{\theta R_0}(\vec{r}, t) \equiv \Psi_v(\vec{r}, t)$. Mathematical proof is absent, but numerical agreement can be pushed to machine precision with relative errors $\sim 10^{-14}$.

These high accuracies can be reached with little effort by infinite range ECS (irECS), where very few ~ 20 discretization coefficients are needed at radii $> R_0$. It consists in using an expansion into spherical harmonics and discretize the radial parts by high order finite elements. As the last element, irECS uses the *infinite* interval $[R_0, \infty)$ and functions of the form $L_n(2\alpha r) \exp(-\alpha r)$ for its discretization, where L_n are Laguerre polynomials. The idea is that low momentum / long de-Broglie wave length electrons need rather large absorption ranges to become absorbed, but that the solution at large distances is rather smooth. The more oscillatory short wave length content of the wave function becomes absorbed within a few oscillations. The exponentially damped functions turned out be very efficient in emulating that behavior: in most cases, about 20 functions at $|\vec{r}| > R_0$ are sufficient for complete absorption. Typical finite element orders used are 15 to 25. The comparatively high order further enhances efficiency of irECS.

Although in irECS there is no strict box boundary, the number of discretization points and the phase space volume that can be represented remain finite. There is a correlation between position discretization and momentum discretization in irECS: large electron momenta can only be represented in the unscaled region and at the beginning of the scaled region. At long distances into the scaled region, only gentle oscillations and therefore low momenta can be represented until the wave function dies out exponentially.

As the finite element basis is local, the discretization coefficients are approximately associated with positions in space. In fact, we can establish a one-to-one relation between the M functions belonging an element and the function values at M different points

within that element. In that sense we will refer to the discretization coefficients as “discretization points”, emphasizing the locality of the finite element functions.

The exact choice of the scaling parameters θ , R_0 and α is not critical. In Ref. [16] we found little variation of accuracy for values in the intervals $\theta \sim [0.5, 0.9]$ and $\alpha \sim [0.2, 0.6]$. Variations of the results with R_0 , as a rule, reflect the spatial discretization error of the calculation. We found this behavior confirmed also for calculation of the photo-electron spectra presented here. The plots shown below were all calculated with $\theta = \alpha = 0.5$.

4. Photo-electron momentum spectra for a short range potential

We solve the time-dependent Schrödinger equation in velocity gauge

$$i \frac{d}{dt} \Psi_v(\vec{r}, t) = \left\{ \frac{1}{2} [-i\vec{\nabla} - \vec{A}(t)]^2 + V(\vec{r}) \right\} \Psi_v(\vec{r}, t) \quad (19)$$

where we first use the short-range “Coulomb” potential

$$V(r) = \begin{cases} c [-1/r - r^2/(2R^3) + 3/(2R)] & \text{for } r \leq R \\ 0 & \text{for } r > R. \end{cases} \quad (20)$$

With $R = 20$ and an effective charge $c = 1.1664$ the ground state energy is -0.5 . The laser pulse is linearly polarized in z -direction with the vector potential

$$A_z(t) = \frac{\mathcal{E}_0}{\omega} \cos^2\left(\frac{\pi t}{2T}\right) \sin(t\omega). \quad (21)$$

We choose parameters $\omega = 0.057$ and $\mathcal{E}_0 = 0.0755$ corresponding to laser wave length of 800 nm and peak intensity $2 \times 10^{14} \text{W/cm}^2$. T is the full width at half maximum (FWHM) of the vector potential, total pulse duration is $2T$.

Figure 1 shows the total and partial wave photo-electron spectra for potential range $R = 20$ and $T = 5$ optical cycles. At these parameters, more than 90% of the electrons get detached. For accuracy $\lesssim 1\%$ up to energies of $10 U_p \approx 120 \text{eV}$ we need $L_{\text{max}} = 30$ partial waves with only 90 radial discretization points. We define the error relative to an accurate reference spectrum σ_{ref} as

$$\mathcal{D}(E) = \frac{|\sigma(E) - \sigma_{\text{ref}}(E)|}{\max(\sigma(E), \langle \sigma(E) \rangle_{\delta E})}, \quad \langle \sigma(E) \rangle_{\delta E} := \frac{1}{2\delta E} \int_{E-\delta E}^{E+\delta E} dE' \sigma(E'). \quad (22)$$

Including in the denominator the average over the interval $[E - \delta E, E + \delta E]$ suppresses spurious spikes in the error due to near-zeros of the spectrum. We choose $\delta E = 0.05 a.u. \approx 1.5 \text{eV}$, which at 800 nm corresponds to averaging over about 2 photo-electron peaks.

In the unscaled region we use 60 points, 30 points are located in $|\vec{r}| > R_0$. The accuracy estimate shown in Fig. 1 is obtained by comparing to a fully converged calculation. When we increase the number of points to 180, the error drops to $\lesssim 10^{-3}$. The increase of relative errors with energy can be attributed to the decrease of the signal: note that from 0 to $10 U_p$ the spectrum drops by more than 5 orders of magnitude.

As a consistency check, we find that spectra up to $10 U_p$ computed with largely different surface radii $R_c = 21$ and 29 coincide within relative accuracies of better than

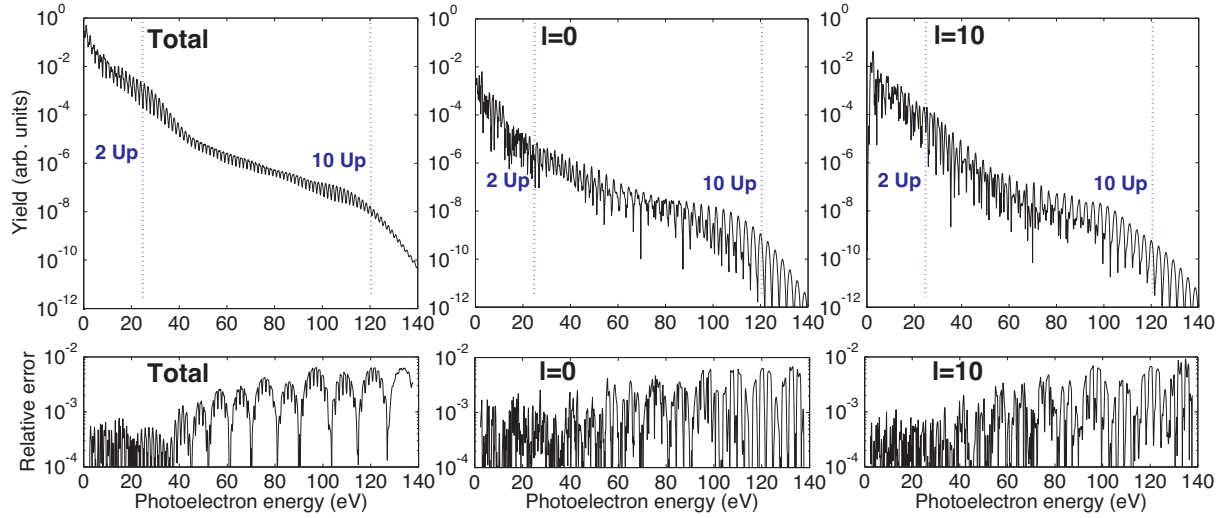


Figure 1. Upper panels: total and partial wave photo-electron spectra obtained for the smoothly truncated Coulomb potential Eq. (20). The lower panels show the relative errors for each spectrum according to Eq. (22) of a calculation with only 90 discretization points per angular momentum comparing to a fully converged calculation. Pulse parameters: $\lambda = 800 \text{ nm}$, $T = 5$ optical cycles, intensity $= 2 \times 10^{14} \text{ W/cm}^2$.

$\lesssim 10^{-3}$. As beyond R_c we assume the exact Volkov propagation, this demonstrates that the solution of the TDSE and the integrals (15) are correct and that also reflections are suppressed on at least that level of accuracy.

The calculated spectra are independent of the complex scaling parameters: over the ranges $R_0 \in [20, 30]$ and $\theta = [0.4, 0.7]$ results vary by less than 10^{-3} . The lower limit for R_0 is not dictated by complex scaling: rather, as we want to obtain exact results, we must pick up the exact wave-function outside the range of the potential $R_c \geq R = 20$, and therefore also $R_0 \geq R_c > R$. Already with these parameters the quiver amplitude, i.e. the excursion of free electrons in the laser field $\mathcal{E}_0/\omega^2 \approx 23$ reaches beyond R_0 and into the complex scaled region. This confirms an earlier observation that the dynamics is correctly reproduced also in the complex scaled region [16].

For correct electron spectra, the effective box size of the combined unscaled and scaled regions must be large enough to accommodate the quiver motion. To study this further, we use a somewhat shorter effective range of $R = 15$ and choose $R_0 = R_c = R$. From Fig. 2 we see that with only 45 discretization point in the unscaled region $r < R_0$ 1% accuracy is reached at the same laser parameters as before. With 30 points for absorptions we have a total of 75 points. Note that the quiver radius of $\approx 23 \text{ a.u.}$ now reaches rather deep into scaled region but still fits into the total box.

Keeping the intensity fixed, a longer wave length of 1000 nm leads to a larger quiver radius of $\approx 36 \text{ a.u.}$ We expect to need a factor $(1000/800)^2 \approx 1.6$ more discretization points. Indeed, we can reach $\lesssim 1\%$ accuracy with total of 120 points in this case (Fig. 2). All additional coefficients and at least half of the quiver motion now are located in the

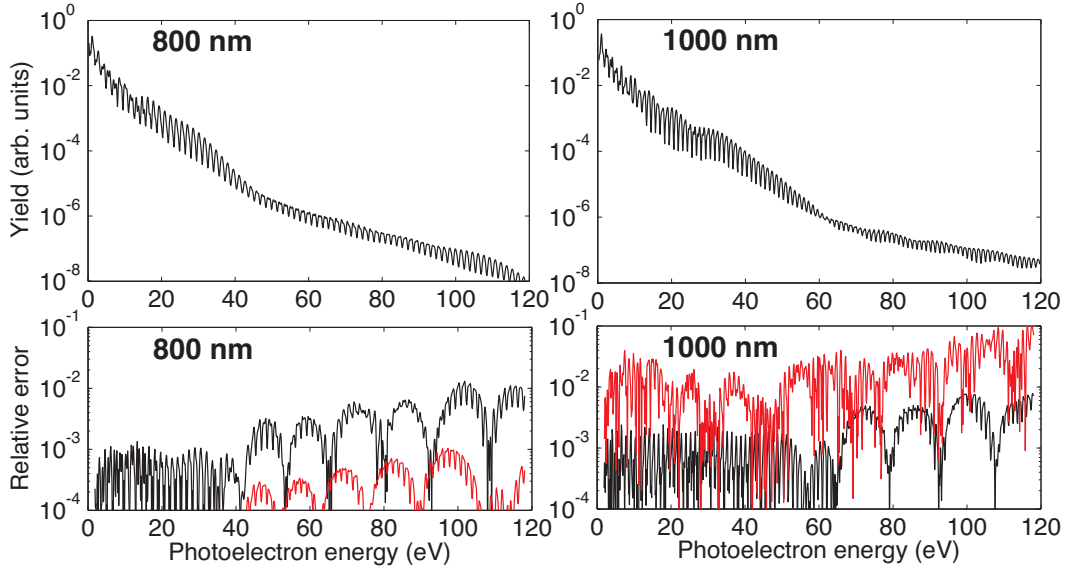


Figure 2. Required box sizes depend on the quiver amplitude. Left panels: spectrum (top) for a 5 cycle FWHM pulse at 800 nm and $\mathcal{E}_0 = 0.0755$ (intensity $2 \times 10^{14} \text{W}/\text{cm}^2$). Accuracies (bottom) are calculated with 75 (black line) and 100 (red line) discretization points. Errors $\lesssim 1\%$ relative to an accurate reference calculation are reached with 75 points. At 100 points the error is $\lesssim 10^{-3}$. Right panels: spectrum (top) and accuracies (bottom) for 5 cycles FWHM at 1000 nm and the same intensity. Because of the larger quiver amplitude, a $\sim 60\%$ larger box with 120 points is needed for $< 1\%$ accurate results. When using a smaller box with 120 points at a 30% higher density errors increase to near 10% (red line).

scaled region. Note that also U_p and with it the peak momentum grows with wave length: for describing the energies $> 120 \text{ eV}$ we would also need to increase the density of points by 25 %. However, just increasing the number of points without increasing the box size gives incorrect results: it appears that we need to accommodate the full quiver motion up to $\sim 36 \text{ a.u.}$ in the simulation box.

5. Photo-electron momentum spectra for the hydrogen atom

As always in scattering problems, the long-range nature of the Coulomb potential introduces extra mathematical and practical complications. Considering *t*-SURFF, there is no surface radius R_c such that the Volkov solutions become exact. In addition, the Rydberg bound states extend to arbitrarily large distances. We will discuss below how these problems can be eliminated with moderate extra computational effort. Here we present the pragmatic solution of using larger R_c such that the remaining error due to the presence of the Coulomb potential becomes acceptable.

Fig. 3 shows a spectrum calculated for the Hydrogen atom with a FWHM $T = 20$ optical cycle pulse at 800 nm wave length and peak intensity $10^{14} \text{W}/\text{cm}^2$. All discretization errors can be controlled in the same way as discussed for the short range

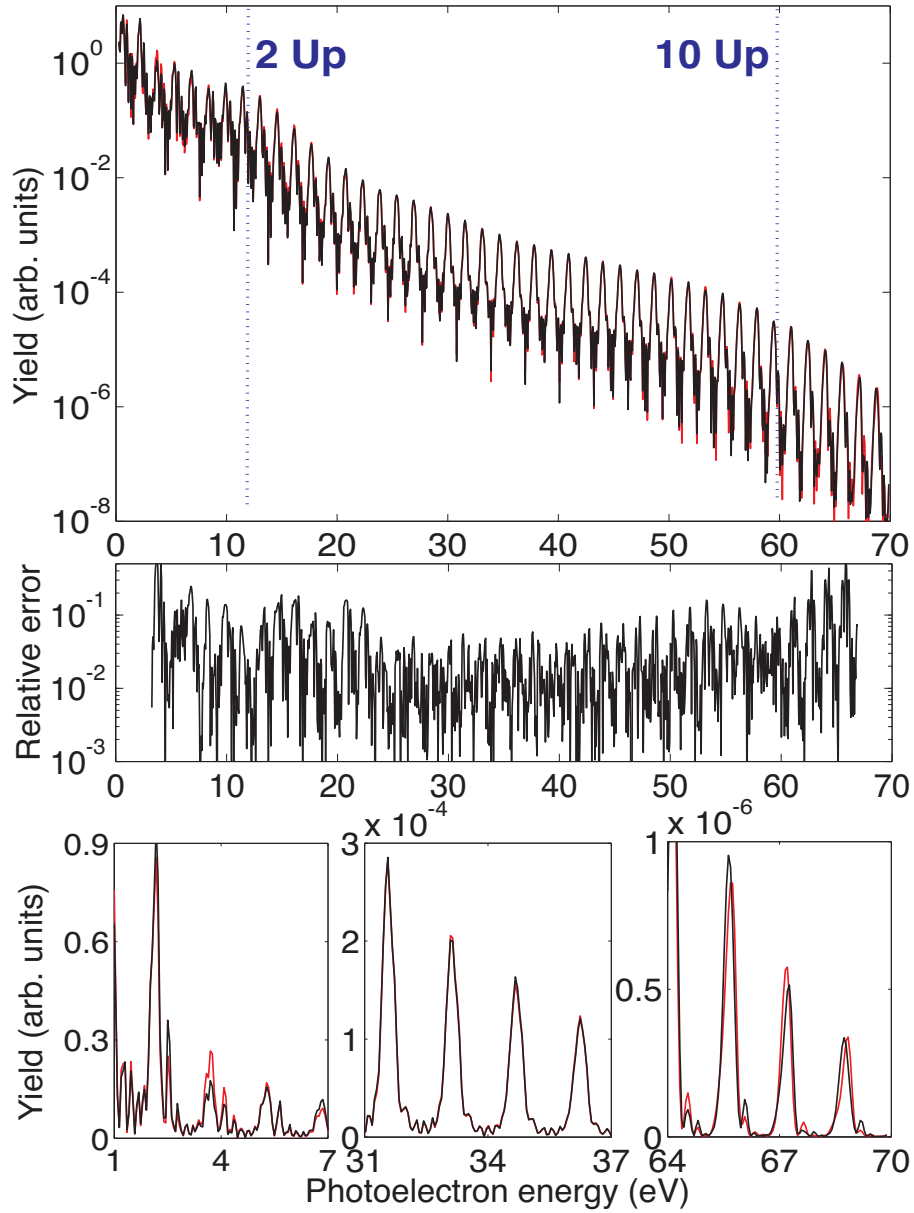


Figure 3. Photo-electron energy spectra for the hydrogen atom (upper panel) obtained with surface radius $R_c = 110$ (black) and $R_c = 140$ (red). Middle panel: error estimate by comparing the spectra according to Eq. (22). Lower panels: blow-up of the spectra from the upper panel on a linear scale. Pulse parameters: $\lambda = 800 \text{ nm}$, $T = 20$ optical cycles, intensity = 10^{14} W/cm^2 .

potential. The error is dominated by the dependence on the surface radius R_c : on an absolute (logarithmic) scale, two calculations with $R_c = 110$ and $R_c = 140$ are hardly discernable. The error level of the calculation with $R_c = 110$ and 180 discretization points is $\lesssim 10\%$ and decreases slowly as R_c increases. In the linear plot of the spectra (lowest panels of Fig. 3) we see that the largest errors occur at lower energies due to the larger influence of the weak Coulomb tail on low energy scattering states. Agreement at intermediate energies is near perfect. The increase of relative errors at the highest energies is due to a displacement of peaks caused slightly incorrect dispersion due to spatial discretization.

Fig. 4 shows angle-resolved photo-electron spectra for FWHM durations of $T=10$, 20 and 30 optical cycles. In the region up to $10 U_p \approx 60 eV$ circular structures with their centers offset along the polarization axis are clearly distinguishable, best visible at the shortest pulse $T = 10$. These structures were first explained in Ref. [17] and are due to re-scattering. The intensity around each circle is related to the electron-ion scattering differential cross section [18]. In the enlarged plots of the energy region up to energies of $2 U_p \approx 12 eV$ we reproduce rings and fan-like structures that are related to particular partial waves, as has been extensively discussed in Ref. [19]. Sub-structures between the photo-electron energy peaks are clearly resolved. These are related to the pulse envelope: the spacing decreases and number of peaks increase as the pulse-duration increases. In different wording one can say that they are caused by interference between rising and trailing edges of the pulse [20].

For comparison with results reported in [9], we also computed the spectrum at the lower intensity of $5 \times 10^{13} W/cm^2$ and $T = 10$ cycles FWHM (corresponding 20 cycles total pulse duration). Fig. 5 shows our result for the total photo-ionization spectrum obtained with only 192 discretization points and 25 angular momenta. We have estimated the accuracy of our results to be $\lesssim 10\%$ throughout the spectrum using the same procedures as for Fig. 3. Our result qualitatively differs from Fig. 2 in Ref. [9], where a surprising irregularity appears near $10 U_p$, while no such structure exists in our spectrum. Unfortunately no detailed discussion of accuracy or convergence is given in [9]. One possible source of the discrepancy is insufficient discretization. With peak energy of $40 U_p \sim 4 a.u.$ included in the calculation the maximal momenta are $p_{\max} \sim 2.8 a.u.$. During 20 optical cycles (2200 a.u. of time), these electrons move to distances $\sim 6000 a.u.$. With the 2000 discretization points used in [9] one gets average momentum grid spacing of $\Delta p = p_{\max}/2000$ and an effective spatial box size $\sim 2\pi/\Delta p \approx 4500$, which appears somewhat below the necessary limit. However, the uneven distribution of grid points and additional spectral cuts in the energy domain used in [9] make it difficult to carry this analysis further. Rather, a systematic convergence study would be required. The present number of discretization points also compares well to the 1000 \sim 2000 discretization coefficients used in [11] at photon energies $0.3 \sim 0.7 a.u.$. The results of the benchmark calculations Refs. [21] obtained with box size of 3000 atomic units and about 4000 discretization points at somewhat shorter wave length of 620 nm could be reproduced using only 200 radial discretization point

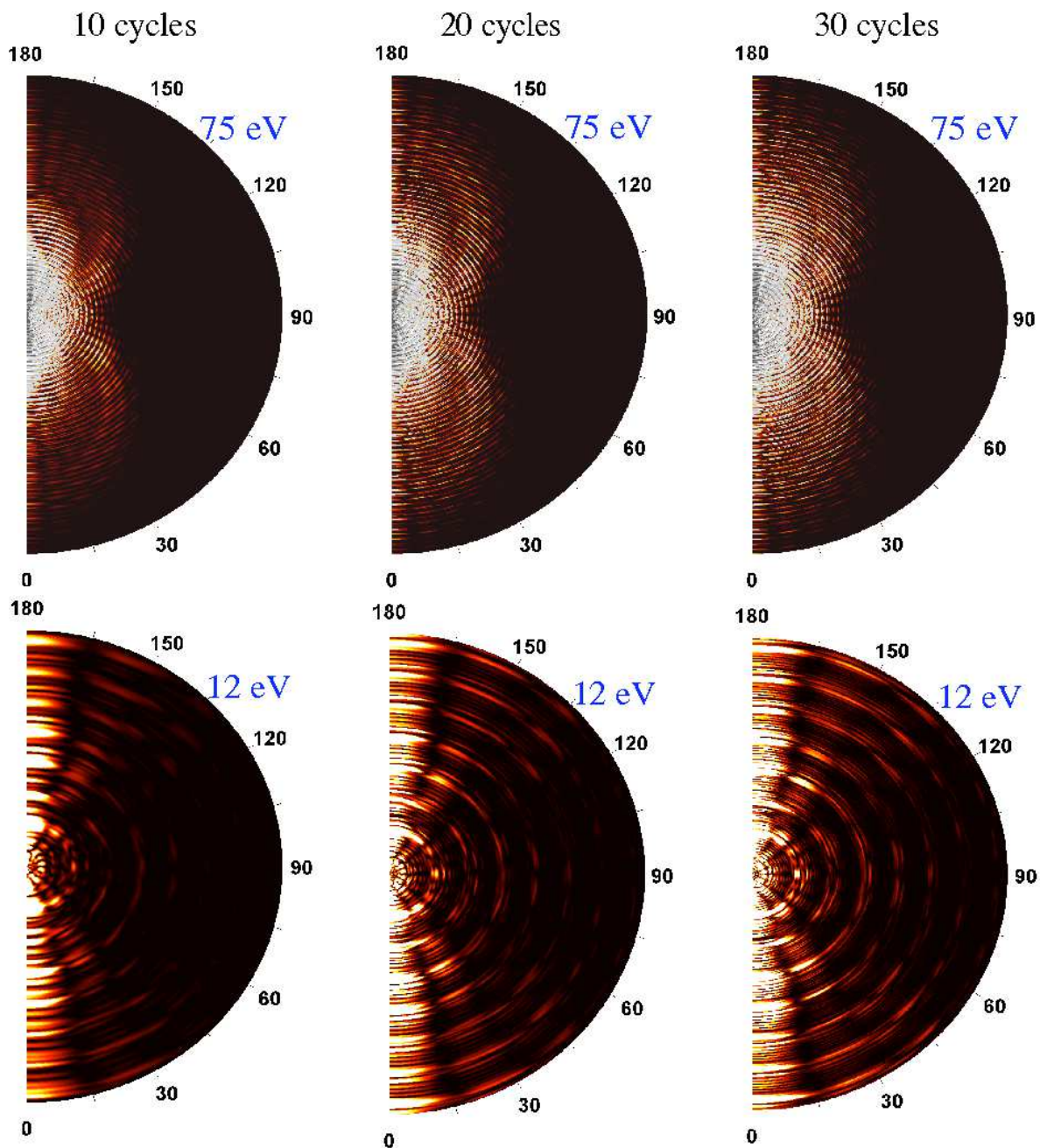


Figure 4. Angle resolved photo-electron energy spectra for the hydrogen atom at $\lambda = 800 \text{ nm}$, intensity 10^{14} W/cm^2 and FWHM pulse durations $T = 10, 20, \text{ and } 30$ (upper panels). In the lower panels, the region up to $2U_p \approx 12 \text{ eV}$ is enlarged.

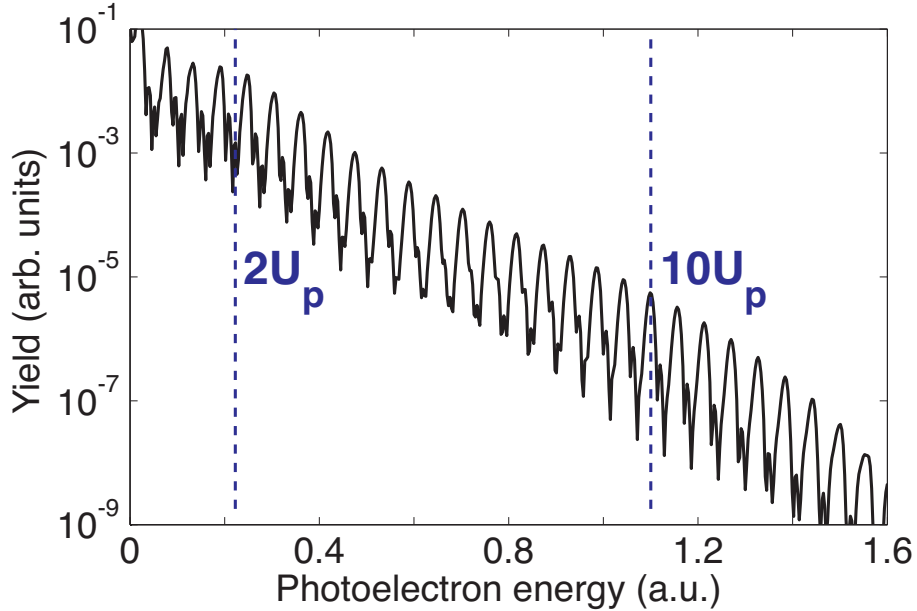


Figure 5. Photo-electron energy spectrum for a FWHM $T = 10$ pulse at 800 nm and peak intensity $I = 5 \times 10^{13} \text{W/cm}^2$. Results obtained with 192 radial discretization points are accurate to a few percent and never exceed 10% in the whole range shown. The pulse parameters agree with those used for Fig. 2 in Ref. [9]. Near $10U_p$ there appears a striking qualitative difference between our result and Ref. [9]. (See text for a discussion.)

up to energies of $10U_p$, except at the lowest energies, where our method is limited by use of Volkov solutions beyond the surface radius $R_c \lesssim 150a.u.$.

6. Extensions of the method

6.1. Handling long-range potentials

In the section above we were able to obtain good results for quite demanding laser parameters using only $R_c \approx 140$. Still, the problem remains big and in particular when considering extension of the approach to multi-electron systems, multi-dimensional simulation volumes would quickly exhaust computational resources. In turn, a reduction of R_c to the necessary minimum of $20 \sim 50$ set by the quiver radius, would constitute an essential gain, possibly deciding about the feasibility of the multi-electron calculation. Here we show how to correctly handle long-range potentials in *t*-SURFF.

For computing exact spectra, we must know the exact solution of the TDSE beyond R_c . In the derivation of Eq. (15) we have only used $H(t) \equiv H_c(t)$ for $|\vec{r}| > R_c$ and that we can by some means obtain accurate solutions $\chi_{\vec{k}}(\vec{r}, t)$ for the TDSE with $H_c(t)$. A suitable H_c is obtained by using in Eq. (19) the potential

$$V_c(r) = \begin{cases} -1/R_c & \text{for } r \leq R_c \\ -1/r & \text{for } r > R_c. \end{cases} \quad (23)$$

Partial wave solutions $\phi_{k,l}(r)$ for the field-free case $\vec{A} \equiv 0$ with V_c are the spherical Bessel functions up to R_c which are connected smoothly to values and derivatives of regular and irregular Coulomb functions in the region $r > R_c$, where one must pay attention to proper δ -normalization. With non-zero field $\vec{\mathcal{E}}(t)$, no exact solution is known. We found that a simple Coulomb-Volkov approximation [22] for the time-dependence is insufficient: we could not observe any acceleration of convergence by replacing the plane waves of the Volkov solution with the field-free scattering solutions. Lacking a reliable approximation for the scattering solution, we must solve the TDSE for the $\chi_{\vec{k}}(\vec{r}, t)$ with the final condition

$$\chi_{k,l}(r, T) = \phi_{k,l}(r). \quad (24)$$

As the potential is weak, little actual scattering occurs and accurate solutions can be obtained by expanding into $\phi_{k',l'}(r)$ for small intervals around the asymptotic radial and angular momenta, $k' \in [k - \Delta k, k + \Delta k]$ and $l' \in [l - \Delta l, l + \Delta l]$. Numerical results using this procedure will be presented elsewhere.

Finally there remains the problem that Rydberg states may become occupied, which have non-negligible amplitude at $r = R_c$. The effect of bound states on the integrals (15) is slow, oscillatory convergence to the asymptotic value at $T \rightarrow \infty$. Again, there is an efficient and rather pragmatic solution to this problem: by averaging the value over several optical cycles, we find that convergence is speeded up and the reported accuracies are reached quickly.

If the Rydberg states are known exactly, we can remove them after the pulse is over. This removes all oscillations and the asymptotic value is reached rapidly. For the procedure we define the projector onto the (field free) Rydberg states $|n\rangle$ and its complement as

$$P := \sum_n |n\rangle\langle n| \text{ and } Q := 1 - P. \quad (25)$$

A simple calculation shows that the spectral amplitude with the Rydberg states removed is

$$\begin{aligned} \langle \chi_{\vec{k}}(T) | \theta(R_c) Q | \Psi(T) \rangle &= i \int_{-\infty}^{T_0} dt \langle \chi_{\vec{k}}(t) | [H_c(t), \theta(R_c)] | \Psi(t) \rangle + \\ & i \int_{T_0}^T dt \langle \chi_{\vec{k}} | [H_c(t), \theta(R_c)] Q | \Psi(t) \rangle - \langle \chi_{\vec{k}}(T_0) | \theta(R_c) P | \Psi(T_0) \rangle, \end{aligned} \quad (26)$$

where T_0 is any time after the end of the pulse. If high precision is wanted and if long time-propagation is costly, the extra effort of implementing the explicit projection (26) may be justified.

6.2. Single-ionization of multi-electron systems

The procedure can be extended to describe single-ionization of multi-electron systems. The main new feature here is that we have several ionization channels, depending on

the state in which the ion is left behind. The spectral density in a specific channel c can be written, as before, as

$$\sigma_c(\vec{k}) = |\langle \chi_{c,\vec{k}}(T) | \theta(R_c) | \Psi_s(T) \rangle|^2. \quad (27)$$

The asymptotic channel wave function $\chi_{c,\vec{k}}(t)$ fullfills the channel TDSE

$$i \frac{d}{dt} \chi_{c,\vec{k}}(t) = H_c(t) \chi_{c,\vec{k}}(t), \quad (28)$$

with the channel Hamiltonian

$$H_c(t) = \frac{1}{2} [-i\vec{\nabla} - \vec{A}(t)]^2 \otimes H_{ion}(t) \quad (29)$$

where for simplicity we neglect the ionic Coulomb potential. Note that we do not need to explicitly anti-symmetrize χ_c , if Ψ_s is anti-symmetric. A general solution of (28) has the form

$$\chi_{c,\vec{k}}(t) = (2\pi)^{-3/2} e^{-i\Phi(t)} e^{i\vec{k}\vec{r}} \otimes \phi_c(t), \quad (30)$$

where $\phi_c(t)$ solves the ionic TDSE with Hamiltonian $H_{ion}(t)$ and a final state condition that specifies the ionic state c of the channel:

$$H_{ion}(T) \phi_c(T) = E_c \phi_c(T). \quad (31)$$

Assuming that double-ionization is negligible, the further steps for computing the spectral amplitude as a time-integral are the same as in the single-electron case. In addition to $\Psi_s(t)$ we must also compute $\phi_c(t)$. Values and derivatives of the c -channel scattering wave function $\varphi_c(\vec{r}, t) := \langle \phi_c(t) | \Psi_s(t) \rangle$ at $|\vec{r}| = R_c$ can be stored for a sufficiently dense time-grid. Because of the stronger binding of electrons in the ion, computing the ionic wave function $\phi_c(t)$ usually requires much less effort than obtaining $\Psi_s(t)$.

6.3. Double-ionization

For double-ionization spectra, we must know the two-electron solution in the asymptotic region. This may be less difficult than what it appears at first glance. Neglecting the ionic potentials, we have a Volkov solution for the center of mass coordinate and Coulomb waves for the relative coordinate. What is left to do is to match that solution with an accurate solution on a five-dimensional surface, where all reflections from the simulation box boundaries are carefully suppressed. While this procedure has not been worked out in detail, it may be well feasible and bring IR two-electron spectra from realm of heroic super-large scale calculations [5] to manageable size, allowing systematic studies.

7. Conclusions and outlook

We have shown that the unfavorable scaling for the computation of photo-electron spectra with laser wave length can be largely overcome with *t*-SURFF, which picks

up the exact solution at some finite surface and beyond that surface exploits knowledge about the long-range behavior of the solutions of the TDSE. The reduction of problem size is particularly striking for atomic binding potentials with finite range, when the Volkov-solutions become exact at distances where the potential is zero. In that case, the box sizes can be reduced to approximately the range of the potential plus the electron quiver amplitude. Electrons that move beyond that range will never scatter and will exactly follow the Volkov solution. For our parameters, the wave function expands to several thousand atomic units during the pulse and correspondingly large boxes would be needed, if a spectral analysis of the wave function were performed after the end of the pulse. In contrast, we could present $\lesssim 1\%$ accurate spectra up to energies of 120 eV using a box size of only about 30 atomic units and as little as 75 discretization points per partial wave. With only a few more points, much higher accuracies can be reached.

Instrumental for the application is the traceless absorption of the wave function beyond the surface, which is provided by the irECS method introduced in a preceding publication [16]. The good performance of irECS for one-dimensional wave functions and for high-harmonic signals from three-dimensional calculations presented in [16] could be confirmed also for the much more delicate observable of angle-resolved photo-electron spectra.

For the long-range Coulomb potential, the Volkov solutions are not exact asymptotically, let alone at any finite distance. In physical language, the electron will scatter in the long-range tail of the Coulomb potential and pick up more energy from the laser field and therefore we cannot predict its final energy before the pulse is over. An attempt to approximate the asymptotic behavior by Coulomb-Volkov instead of the pure Volkov solutions was futile. In a pragmatic approach, we could show that with a surface at distances of $R_c = 100 \sim 140$ atomic units, still impressively accurate spectra can be obtained using Volkov solutions as approximation to the exact asymptotic solutions.

For single-electron systems and with moderate accuracy requirements, simulation volumes on the scale of ~ 100 atomic units are quite acceptable. For experimentally interesting multi-electron systems, we have proposed to further reduce box-sizes by solving the asymptotic laser-assisted scattering problem numerically. This may be done efficiently for an asymptotic Hamiltonian that only includes scattering at distances $> R_c$ and dismisses the main part of scattering from near the Coulomb singularity. The need to solve this weak scattering problem enhances the complexity of coding and significantly increases computation times. However, for few-electron systems, this extra effort is far compensated by an expected reduction to box sizes to as little as $20 \sim 50$ atomic units. We have also formulated the extension of t-SURFF to single- and double-ionization of multi-electron systems. A numerical demonstration of these methods will be the subject of future work.

In summary, t-SURFF, while producing highly accurate results, can reduce the box size for computing IR photo-electron spectra for single electron systems by one order of magnitude or more. This drastic reduction of box-sizes is particularly important for very long laser wave length and for multi-electron systems. For systems with two and

more electrons, we believe, it opens a route to computing accurate IR photo-electron momentum spectra.

Acknowledgments

This work has been supported by the Austrian Science Fund within the framework of the Special Research Program F41 Vienna Computational Materials Laboratory (ViCoM).

References

- [1] P. B. Corkum. Plasma perspective on strong-field multiphoton ionization. *Phys. Rev. Lett.*, 71:1994, 1993.
- [2] M. Spanner, O. Smirnova, P. Corkum, and M. Ivanov. Reading diffraction images in strong field ionization of diatomic molecules. *J. Phys. B*, 37:L243, 2004.
- [3] S. N. Yurchenko, S. Patchkovskii, I. V. Litvinyuk, P. B. Corkum, and G. L. Yudin. Laser-induced interference, focusing, and diffraction of rescattering molecular photoelectrons. *Phys. Rev. Lett.*, 93:223003, 2004.
- [4] M. Meckel, D. Comtois, D. Zeidler, A. Staudte, D. Pavicic, H. C. Bandulet, H. Pepin, J. C. Kieffer, R. Doerner, D. M. Villeneuve, and P. B. Corkum. Laser-induced electron tunneling and diffraction. *Science*, 320(5882):1478–1482, Jun 13 2008.
- [5] KT Taylor, JS Parker, KJ Meharg, and D Dundas. Laser-driven helium at 780 nm. *Eur. Phys. J. D*, 26(1):67–71, OCT 2003.
- [6] F. Martin, J. Fernandez, T. Havermeier, L. Foucar, Th. Weiber, K. Kreidi, M. Schoeffler, L. Schmidt, T. Jahnke, O. Jagutzki, A. Czasch, E. P. Benis, T. Osipov, A. L. Landers, A. Belkacem, M. H. Prior, H. Schmidt-Boecking, C. L. Cocke, and R. Doerner. Single photon-induced symmetry breaking of H-2 dissociation. *Science*, 315(5812):629–633, 2007.
- [7] E Cormier and P Lambropoulos. Optimal gauge and gauge invariance in non-perturbative time-dependent calculation of above-threshold ionization. *J. Phys. B*, 29(9):1667–1680, May 14 1996.
- [8] Dmitry A. Telnov and Shih-I Chu. Above-threshold-ionization spectra from the core region of a time-dependent wave packet: An ab initio time-dependent approach. *Phys. Rev. A*, 79(4), APR 2009.
- [9] Zhongyuan Zhou and Shih-I Chu. Precision calculation of above-threshold multiphoton ionization in intense short-wavelength laser fields: The momentum-space approach and time-dependent generalized pseudospectral method. *Phys. Rev. A*, 83(1), Jan 19 2011.
- [10] A. Scrinzi, T. Brabec, and M. Walser. 3d numerical calculations of laser-atom interactions. In B. Piraux and K. Rzaszewski, editors, *Proceedings of the Workshop Super-Intense Laser-Atom Physics*, page 313. Kluwer Academic Publishers, 2001.
- [11] Aliou Hamido, Johannes Eiglsperger, Javier Madronero, Francisca Mota-Furtado, Patrick O’Mahony, Ana Laura Frapiccini, and Bernard Piraux. Time scaling with efficient time-propagation techniques for atoms and molecules in pulsed radiation fields. *Phys. Rev. A*, 84(1), Jul 27 2011.
- [12] G. G. Balint-Kurti, R. N. Dixon, C. C. Marston, and A. J. Mulholland. The calculation of product quantum state distributions and partial cross-sections in time-dependent molecular collision and photodissociation theory. *Comp. Phys. Comm.*, 63:126, 1991.
- [13] David J. Tannor and David E. Weeks. Wave packet correlation function formulation of scattering theory: The quantum analog of classical s-matrix theory. *J. Chem. Phys.*, 98:3884, 1993.
- [14] Jeremie Caillat, Jürgen Zanghellini, Markus Kitzler, Othmar Koch, Wolfgang Kreuzer, and Armin Scrinzi. Correlated multielectron systems in strong laser fields - an mctdhf approach. *Phys. Rev. A*, 71:012712, 2005.

- [15] J.G. Muga, J.P. Palao, B. Navarro, and I.L. Egusquiza. Complex absorbing potentials. *Physics Reports*, 395(6):357 – 426, 2004.
- [16] Armin Scrinzi. Infinite-range exterior complex scaling as a perfect absorber in time-dependent problems. *Phys. Rev. A*, 81(5):053845, May 2010.
- [17] Toru Morishita, Anh-Thu Le, Zhangjin Chen, and C. D. Lin. Accurate retrieval of structural information from laser-induced photoelectron and high-order harmonic spectra by few-cycle laser pulses. *Phys. Rev. Lett.*, 100:013903, Jan 2008.
- [18] Zhangjin Chen, Anh-Thu Le, Toru Morishita, and C. D. Lin. Quantitative rescattering theory for laser-induced high-energy plateau photoelectron spectra. *Phys. Rev. A*, 79:033409, Mar 2009.
- [19] Toru Morishita, Zhangjin Chen, Shinichi Watanabe, and C. D. Lin. Two-dimensional electron momentum spectra of argon ionized by short intense lasers: Comparison of theory with experiment. *Phys. Rev. A*, 75:023407, Feb 2007.
- [20] D A Telnov and S I Chu. Multiphoton above-threshold detachment by intense laser pulses: a new adiabatic approach. *Journal of Physics B: Atomic, Molecular and Optical Physics*, 28(12):2407, 1995.
- [21] E Cormier and P Lambropoulos. Above-threshold ionization spectrum of hydrogen using B-spline functions. *J. Phys. B*, 30(1):77–91, JAN 14 1997.
- [22] G. Duchateau, E. Cormier, and R. Gayet. Coulomb-volkov approach of ionization by extreme-ultraviolet laser pulses in the subfemtosecond regime. *Phys. Rev. A*, 66:023412, 2002.